Highly Selective Electrocatalytic CuEDTA Reduction by MoS$_2$ Nanosheets for Efficient Pollutant Removal and Simultaneous Electric Power Output

Hehe Qin[1,2], Xinru Liu[1,2], Xiangyun Liu[1,2], Hongying Zhao[3], Shun Mao[1,2] ✉

HIGHLIGHTS

- Highly efficient CuEDTA removal by an electrolyzer with MoS$_2$ nanosheet cathode.

- Higher removal rate and Faraday efficiency compared with other widely reported electrocatalytic technologies.

- CuEDTA/Zn primary battery is constructed for the first time to realize CuEDTA removal and synchronous power generation.

ABSTRACT Electrocatalytic reduction of ethylenediamine tetraacetic acid copper (CuEDTA), a typical refractory heavy metal complexation pollutant, is an environmental benign method that operates at mild condition. Unfortunately, the selective reduction of CuEDTA is still a big
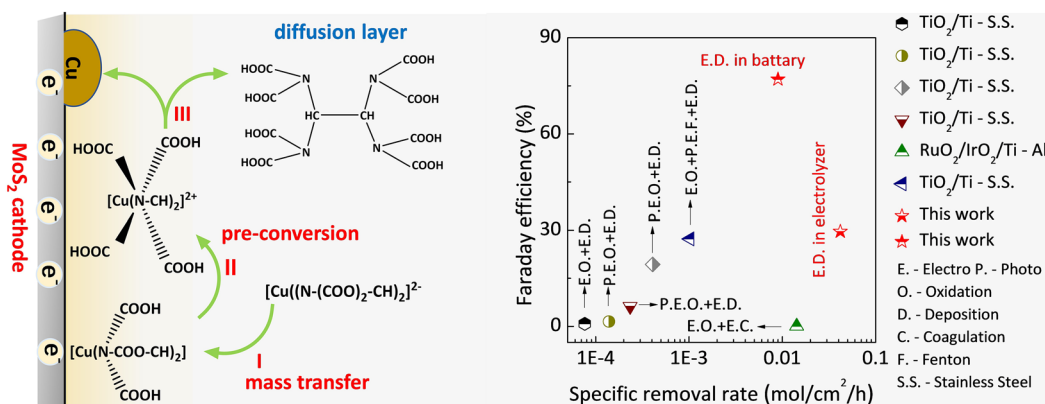
challenge in cathodic process. In this work, we report a MoS$_2$ nanosheet/graphite felt (GF) cathode, which achieves an average Faraday efficiency of 29.6% and specific removal rate (SRR) of 0.042 mol/cm^2/h for CuEDTA at −0.65 V vs SCE (saturated calomel electrode), both of which are much higher than those of the commonly reported electrooxidation technology-based removal systems. Moreover, a proof-of-concept CuEDTA/Zn battery with Zn anode and MoS$_2$/GF cathode is demonstrated, which has bifunctions of simultaneous CuEDTA removal and energy output. This is one of the pioneer studies on the electrocatalytic reduction of heavy metal complex and CuEDTA/Zn battery, which brings new insights in developing efficient electrocatalytic reduction system for pollution control and energy output.

KEYWORDS Electrocatalytic reduction; CuEDTA removal; MoS$_2$ nanosheet; CuEDTA/Zn battery; Faraday efficiency

✉ Shun Mao, shunmao@tongji.edu.cn

[1] College of Environmental Science and Engineering, Biomedical Multidisciplinary Innovation Research Institute, Shanghai East Hospital, State Key Laboratory of Pollution Control and Resource Reuse, Tongji University, 1239 Siping Road, Shanghai 200092, People's Republic of China

[2] Shanghai Institute of Pollution Control and Ecological Security, Shanghai 200092, People's Republic of China

[3] Shanghai Key Lab of Chemical Assessment and Sustainability, School of Chemical Science and Engineering, Tongji University, 1239 Siping Road, Shanghai 200092, People's Republic of China

1 Introduction

Ethylenediamine tetraacetic acid copper (CuEDTA), one of the typical refractory and toxic heavy metal complexation pollutants, is massively discharged from industrial processes including electroplating and metallurgy [1]. The extremely stable structure and highly soluble property of CuEDTA over a wide pH range make it quite challenge to apply the traditional precipitation treatment method for this heavy metal complexation [2]. On the other hand, as a valuable metal, the recovery of Cu from CuEDTA wastewater is important for both resource utilization and pollution control [3, 4]. To realize the treatment and recovery of the complexes, a common strategy is decomplexation by oxidation coupled with the deposition of metal [2, 3, 5–13]. However, obstacles of high energy consumption and low removal or recovery rate/ efficiency prevent the practical applications of this method. For instance, Wang et. al. reported the oxidative decomplexation of CuEDTA by HCO_3^-/H_2O_2-based advanced oxidation technique, which required ~2000 times of H_2O_2 dosage to achieve 40–92% decomplexation and 74.8% total organic carbon (TOC) removal of 0.2 mM CuEDTA in 60 min [14]. Therefore, more efficient technology for metal–organic complex removal is highly needed.

Electrochemical reduction is an electrode interface reaction process, in which the reactant gains electrons directly at the electrode, and the reaction proceeds at a certain rate when an appropriate overpotential is applied [15, 16]. Cathodic reduction has unique advantage in CuEDTA removal since Cu is directly precipitated by cathodic reduction through a two-electron process of the central Cu^{2+} without ligand degradation [17]. Then, the de-complexed EDTA can either be recycled or removed using less costly biological treatment techniques, which shows lower energy consumption than that of the anodic decomplexation/precipitation process [17, 18]. Direct electrochemical reduction of CuEDTA has been reported in previous studies [17–21]. However, these studies mainly focus on the operation parameter optimizations in the reactor including solution pH, electrolyte, current density, flow rate, etc. Although high Cu recovery efficiency can be achieved in these systems, the current efficiency is relatively low (25%) even with CuEDTA concentrations up to 10 mM [17, 21], which greatly limits the practical applications of this technology due to the unaffordable energy consumption. Another important issue in electrochemical reduction of

CuEDTA is that the hydrogen evolution reaction (HER) at the cathode is ignored in most cases, which is a competitive reaction for CuEDTA reduction reaction (CuRR) in cathodic reaction. To address these challenges, highly selective and efficient cathode for CuRR is needed to realize the practical applications of this technology.

2D MoS_2 nanosheet (NS) has exposed edges and basal plane, which shows unique surface chemistry properties compared with its bulk form [22, 23]. MoS_2 nanosheets have been reported in electrocatalytic reactions including N_2 or NO reduction reaction [24–26], CO_2 reduction reaction [27], O_2 reduction reaction [28, 29], etc. In one study, Zhang et al. reported the electrochemical reduction of NO on MoS_2 (1 0 1) crystalline surface. They showed that MoS_2 was more conducive to NO adsorption, and the N–O bond of adsorbed NO was elongated, which benefited the subsequent electroreduction process [24]. Motivated by these studies, we speculate that MoS_2 nanosheet may have promising catalytic activity in cathodic reduction of CuEDTA.

In this work, we report a MoS_2 nanosheet-based electrode with abundant exposed edges for selective CuEDTA reduction. This cathode achieves high catalytic performance for CuRR, which is superior to commonly used cathodes in electrocatalytic systems including Pt/C, Cu, and carbon black [30]. Based on the density functional theory (DFT) modeling, it is shown that the activation energy of CuRR on the MoS_2 surface is 0.114 eV, which is much lower than that of the graphite electrode (0.821 eV). Considering the outstanding activity of MoS_2 nanosheet for CuRR, two types of electrochemical devices, i.e., electrolyzer and CuEDTA/ Zn battery, are constructed and demonstrated by the MoS_2/ graphite felt (GF) cathode. In the electrolyzer, the MoS_2/GF achieves an average Faraday efficiency (FE) of 29.6% and a high specific removal rate (SRR) of 0.042 mol cm^{-2} h^{-1} for CuEDTA at −0.65 V versus SCE, both of which are higher than those of the (photo)electrooxidation technology-based removal systems [3, 31]. In the CuEDTA/Zn battery, a maximum power density of 1.05 mW cm^{-2} at 1.95 mA cm^{-2} can be delivered. The MoS_2/GF cathode battery can achieve 75% removal of CuEDTA with a superhigh FE of 77%. To the best of our knowledge, this is the first report of CuRR coupled with battery application for the CuEDTA treatment and energy storage. The reported highly efficient and low energy consumption electrolyzer for CuEDTA removal and CuEDTA/Zn battery present new insights in the practical

applications of electrochemical system for heavy metal complex treatment and energy reuse.

2 Experimental

2.1 Preparation of MoS$_2$/GF Cathode

The MoS$_2$/GF cathode was prepared by the hydrothermal synthesis method. In detail, 1 mmol Na$_2$MoO$_4$ and 5 mmol urea were dissolved in 30 mL ultrapure water. The GF (6 cm × 2 cm) was washed with dichloromethane, ethanol, and 0.1 M hydrochloric acid, successively. Then, the mixed liquor was transferred into a Teflon-lined stainless-steel autoclave. The washed GF was rolled and placed into the autoclave. After 24 h hydrothermal reaction at 200 °C, the MoS$_2$ nanosheets were produced and deposited on the GF surface. The MoS$_2$/GF was dried in vacuum and cut into small pieces for later use.

2.2 CuEDTA Removal by Electrolyzer

The CuEDTA electroreduction experiment was carried out in the two-compartment reaction cell separated by the ion exchange membrane. The MoS$_2$/GF was used as the cathode (size of 3 cm^2) and Pt plate was used as the anode. The CuEDTA (1 mM) and Na$_2$SO$_4$ (0.5 M) was used as the electrolyte for the cathode and anode compartment, respectively, and the solution volume was 30 mL for each compartment. A polymer electrolyte membrane (PEM) was used to separate the cathode and anode. During the reaction, at a predetermined sampling time, 0.25 mL reaction solution was collected and diluted with 0.25 mL H$_2$O for real-time CuEDTA concentration determination or 0.25 mL of 1 mM CuSO$_4$ solution for total CuEDTA concentration determination by high-performance liquid chromatography test (HPLC, Agilent 1260, USA). The real-time concentration of EDTA was obtained by subtracting the real-time CuEDTA from the total concentration. The test conditions of HPLC were as follows: the test wavelength was 225 nm, the column was C$_{18}$ (4.6 × 250 mm), the volume ratio of 10 mM H$_3$PO$_4$ to acetonitrile water was 92:8, and the flow rate was 1 mL min^{-1}. The standard curve of CuEDTA concentration determined by HPLC is shown Fig. S1. The electrode regeneration was achieved by soaking the Cu-deposited MoS$_2$/GF in saturated ethylenediamine tetraacetic acid for 24 h. Tap water and surface water (filtered by 0.44 μm water phase needle filter, from Tongji University campus) were used to study the impact of coexist chemicals in real water samples on the electroreduction efficiency of CuEDTA in our system.

2.3 CuEDTA/Zn Battery Test

The CuEDTA/Zn battery was constructed in the two-compartment reaction cell separated by the bipolar ion exchange membrane (BIEM). The MoS$_2$/GF was used as the cathode (size of 3 cm^2) and Zn plate was used as the anode. The Na$_2$SO$_4$ (0.5 M) and KOH (1 M) was used as the electrolyte for the cathode and anode compartment, respectively, and the solution volume was 30 mL for each compartment. The output characteristics of the battery were measured by chronopotentiometry with current ramp method, and the current sweep speed was 0.1 mA s^{-1}. The CuEDTA concentration was measured with the same method using HPLC. Chronopotentiometry was used to measure the potential change under constant current discharge condition. In both electrolyzer and battery cells, Ar was continuously pumped to prevent interference of oxygen and carbon dioxide in the air. Other experimental details of material characterizations and electrochemical tests are shown in the Supporting Information (Text S2–S3).

3 Results and Discussion

3.1 Reactor Design and Electrode Characterizations

Figure 1a shows the experimental device used in this study, which is a two-compartment reaction cell separated by an ion exchange membrane. The core reaction of the reactor is the CuRR on the cathode, which occurs in both electrolyzer and primary battery. With the MoS$_2$/GF cathode, the CuEDTA decomplexation and reduction proceed to produce copper deposition on the cathode surface (Fig. 1b). In the electrolytic cell system, the CuEDTA is removed and Cu is recovered by the applied voltage; while the oxygen evolution occurs at the counter electrode (Fig. 1c). In the CuEDTA/Zn battery, the redox reaction between Zn and CuEDTA occurs spontaneously and generates electrical energy (Fig. 1d). In order to eliminate the interference of oxygen and other reactive gases, the devices were operated under the protection of argon.

The prepared MoS$_2$ nanosheets with exposed edges on the GF electrode are first characterized. As shown in the
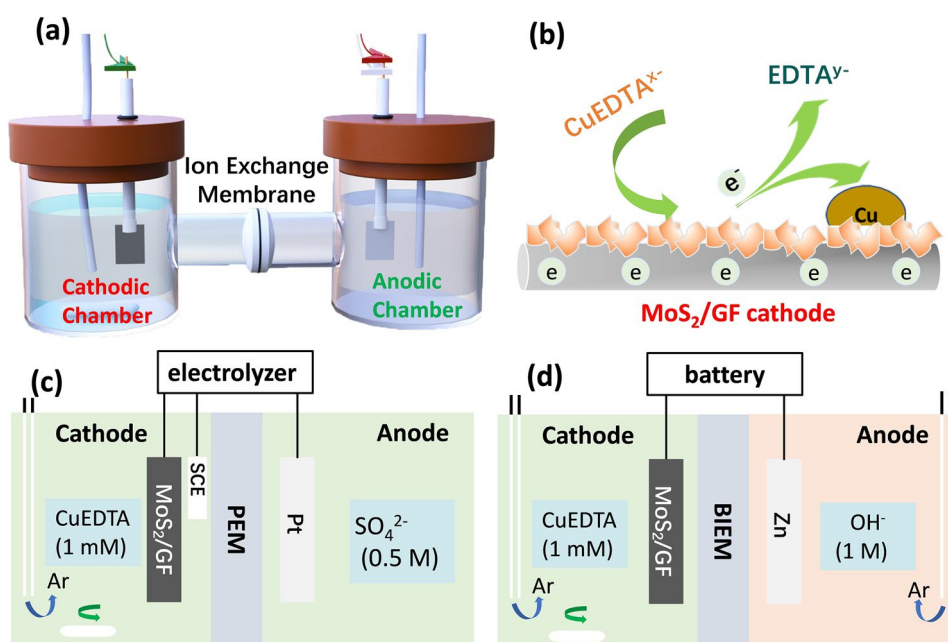
Fig. 1 **a** Schematic diagram of the reaction system. **b** CuEDTA reduction reaction on the MoS_2/GF cathode. **c, d** Schematic diagrams of the electrolyzer and CuEDTA/Zn battery

scanning electron microscope (SEM) image, the GF electrode has a smooth surface (Fig. 2a). After the in-situ synthesis of MoS_2 nanosheets, the GF is fully covered by a dense MoS_2 layer (Fig. 2b). The nanosheet feature is evidenced by the transmission electron microscope (TEM) image shown in Fig. 2c, which indicates that the MoS_2 nanosheets have a vertically-aligned structure with large number of exposed edges. The high-resolution TEM (HRTEM) image (Fig. 2d) and selected area electron diffraction (SAED) patterns (Fig. 2e) confirm the crystalline structure of MoS_2. The 0.258 nm lattice fringe in the HRTEM image can be indexed to the (1 0 1) crystal plane of hexagonal MoS_2 crystalline.

The X-ray diffraction (XRD) patterns in Fig. 2f show diffraction peaks at 13.9°, 33.0°, and 58.0°, which may be attributed to the diffraction peaks of polytype 2H-MoS_2 or 3R-MoS_2 [32, 33]. The Raman spectroscopy was further obtained to investigate the structure of the prepared MoS_2 nanosheet (Fig. S2). The MoS_2 nanosheet exhibits two vibration bands at 385 cm^{-1} (E_{2g}) and 405 cm^{-1} (A_{1g}), which demonstrates that the 2H-MoS_2 phase is the major constituent [34]. The energy dispersive spectroscopy (EDS) spectrum of the prepared MoS_2 nanosheet is shown in Fig. S3. In addition to Mo and S, there is also a certain amount of C, which may be attributed to the carbon

in the organic thiourea from which MoS_2 is synthesized. The atomic ratio of S to Mo is measured as 1.95, further confirming the successful preparation of MoS_2.

The surface chemical states of MoS_2 were characterized by X-ray photoelectron spectroscopy (XPS). As shown in Fig. S4, the peaks at 236.0, 232.8, and 229.3 eV can be attributed to Mo(VI) $3d_{3/2}$ of MoS_2 surface plasmon, Mo(IV) $3d_{3/2}$ and Mo(IV) $3d_{5/2}$ of MoS_2, respectively. The extra peak at ~ 226.3 eV in Mo 3d XPS is referred as S 2s. The peak at 162.3 eV corresponds to Mo^+ state in S $2p_{3/2}$, and the peaks at 163.3 and 169 eV are Mo^{2+}/MoS_2 surface plasmon state in S $2p_{1/2}$. The XPS results are consistent with the reported electronic structure of 2D MoS_2 thin film [35].

3.2 Electrochemical Characterizations and CuRR Mechanism

Before the device demonstration of the electrochemical CuEDTA removal, electrochemical characterizations were performed to study the electrode process of CuRR on the MoS_2 cathode. The catalytic activity of the prepared catalyst towards CuRR in 0.5 M Na_2SO_4 solution was firstly evaluated by cyclic voltammetry (CV) measurements
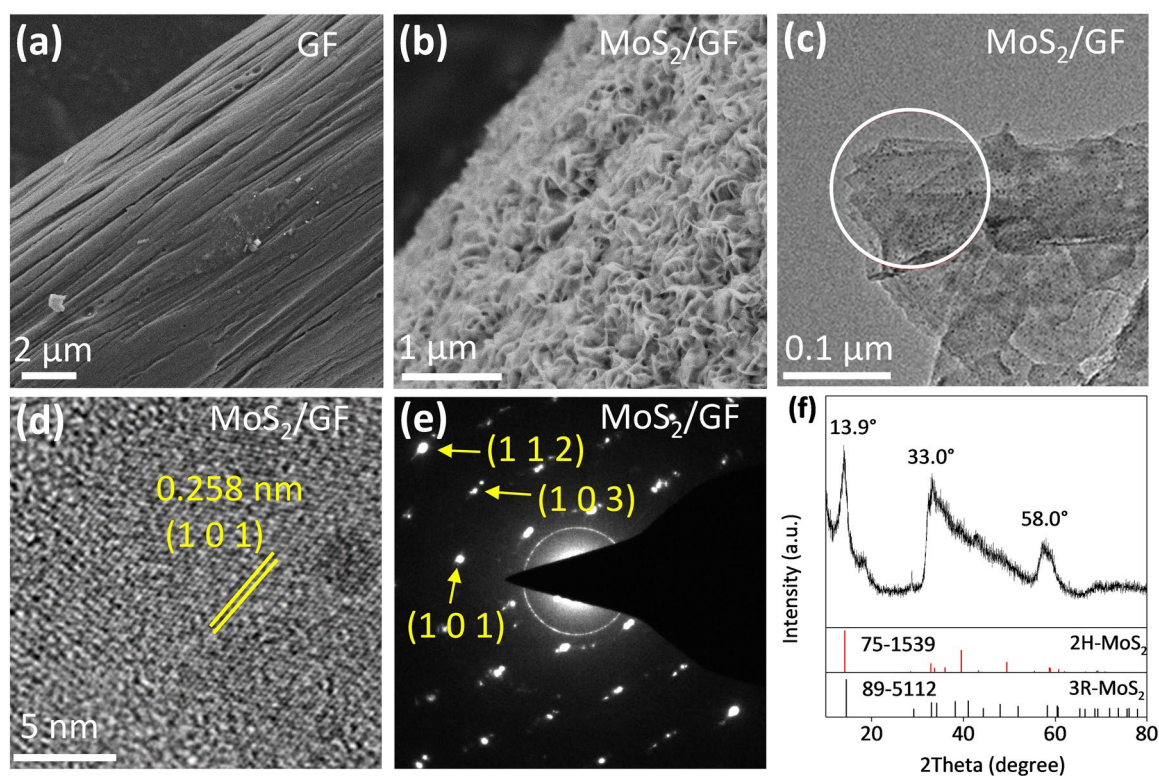
Fig. 2 SEM images of **a** bare GF and **b** MoS_2/GF. **c** TEM and **d** HRTEM images of MoS_2 nanosheet. **e** The corresponding SEAD patterns of MoS_2 in the circle location of **c**. **f** XRD patterns of MoS_2

(Fig. S5). For comparison, the voltammograms of commonly used Pt/C, Cu, carbon black (CB), and glassy carbon (GC) electrodes in electrochemical reduction territory were also tested. Compared with the CV curves recorded in the Na_2EDTA solution (red curve), the redox currents were observed for MoS_2 electrode, while the other electrodes showed no obvious redox currents, indicating that the MoS_2 nanosheet has superior catalytic activity for CuRR.

As shown in Fig. 3a, the linear sweep voltammetry (LSV) curves further indicate that the MoS_2 cathode has higher electrochemical activity for CuRR, and its reduction current exceeds those of the Pt/C, Cu, CB, and GC electrodes. Since the thermodynamic standard potential of CuEDTA reduction is lower than that of HER (Text S1), it is inevitable that the CuRR and HER will occur simultaneously. Thus, we further compared the HER and CuRR currents of the MoS_2 cathode to investigate its activity and selectivity for these two competing reactions.

For the MoS_2 electrode, Fig. 3b clearly shows that the reduction current of CuRR (10 mM CuEDTA) is greater than that of HER (10 mM Na_2EDTA), indicating that MoS_2

nanosheet cathode has a strong selectivity for CuRR over HER. In contrast, the other cathodes show different activities in CuRR and HER. As shown Fig. S6, the HER performance is excellent for Pt/C. However, the cathodic current is greatly inhibited in the presence of CuEDTA, which indicates that the Pt/C cathode has an intrinsic inferior activity of CuRR compared with HER. As for Cu cathode, the similar decrease in current density is found in the presence of CuEDTA, which may also be ascribed to the inherent lower catalytic activity for CuRR than HER. No difference is observed between the HER and CuRR currents on the CB cathode since the activity of CB cathode is low for both reactions. The above results indicate that MoS_2 nanosheet has the strongest CuRR selectivity among the studied cathodes.

The limit current of CuRR on MoS_2 cathode can be used to verify if the reaction is controlled by non-electron-transfer steps like mass transfer or pre-conversion steps. Hence, we carried out rotating disk electrode tests at different rotate speeds to reveal if the CuRR on MoS_2 electrode was controlled by the mass transfer step. As shown in Fig. 3c, the limit current density of CuRR increases with the increased
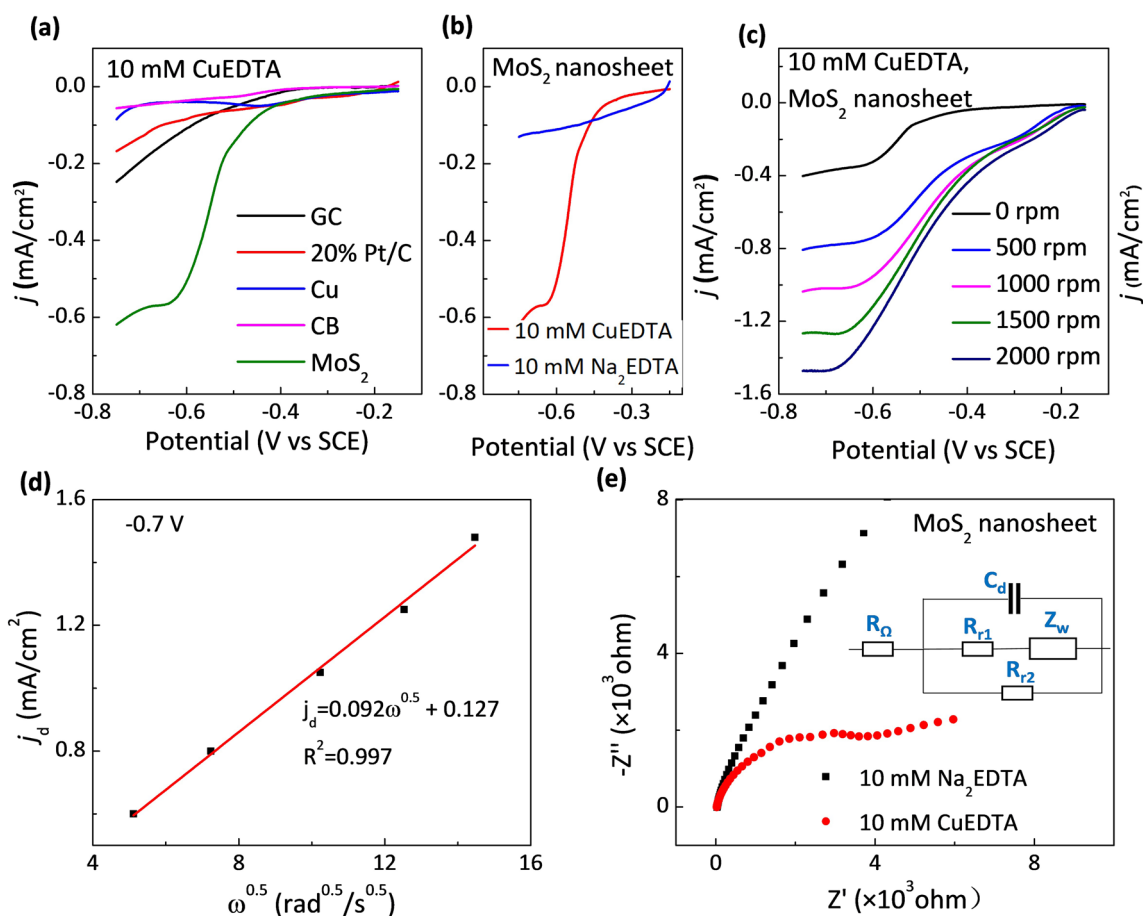
Fig. 3 **a** LSVs of different cathodes for CuRR (10 mM CuEDTA, rotation speed of 250 rpm). **b** LSVs of the MoS$_2$/GF cathode for HER (10 mM Na$_2$EDTA, rotation speed of 250 rpm) and CuRR (10 mM CuEDTA, rotation speed of 250 rpm). **c** LSVs of the MoS$_2$/GF cathode for CuRR at different rotation speeds. **d** $j_d - \omega^{1/2}$ plot at -0.75 V versus SCE. **e** Nyquist plots of the MoS$_2$ cathode for CuRR and HER at -0.75 V versus SCE. The inset shows the equivalent circuit of the electrochemical system. C_d is the differential capacitance, R is the solution resistance (R_Ω) or reaction resistance (R_{r1} and R_{r2}), and Z_w is the electrochemical reaction and mass transfer complex impedance

rotation speed, indicating that, in the tested potential range and rotation speed, the CuEDTA reduction reaction is controlled by the mass transfer process. Similarly, we have also carried out the rotating disk tests on the other cathodes (Fig. S6). Different from the results on MoS$_2$ cathode, no difference was observed at various rotation speeds, indicating the non-mass-transfer controlled reaction current and their limited electrocatalytic reduction performances. The high catalytic activity and selectivity of the MoS$_2$ cathode for CuRR can also be confirmed from the Nyquist plots (Fig. 3e), which shows smaller radius of curvature for CuRR compared with that of HER. On the other reference electrodes, there is no significant difference in the reaction resistance between HER and CuRR (Fig. S7). In addition, according to the fitting curve of the relationship between

the limiting current density (j_d) and the rotational angular velocity ($\omega^{1/2}$) in Fig. 3d, the electron transfer number is calculated to be ~ 1.9, indicating that the two-electron CuRR process is the main process in the system.

Figure 4a shows the schematic diagram of electrocatalytic reduction process of CuEDTA at the MoS$_2$ cathode. For the electrocatalytic CuEDTA reduction, the first step is the mass transfer process of the CuEDTA to the cathode surface. Based on the above electrochemical test results, we have shown that CuRR is limited by the mass transfer on MoS$_2$ cathode; while the CuRR on the other cathodes is limited by their inherently poor catalytic activity in the pre-conversion step under good mass transfer conditions (Text S5). In general, the vacant orbital of the central metal ion of the coordination compound is filled with lone pair electrons of the ligands; while,
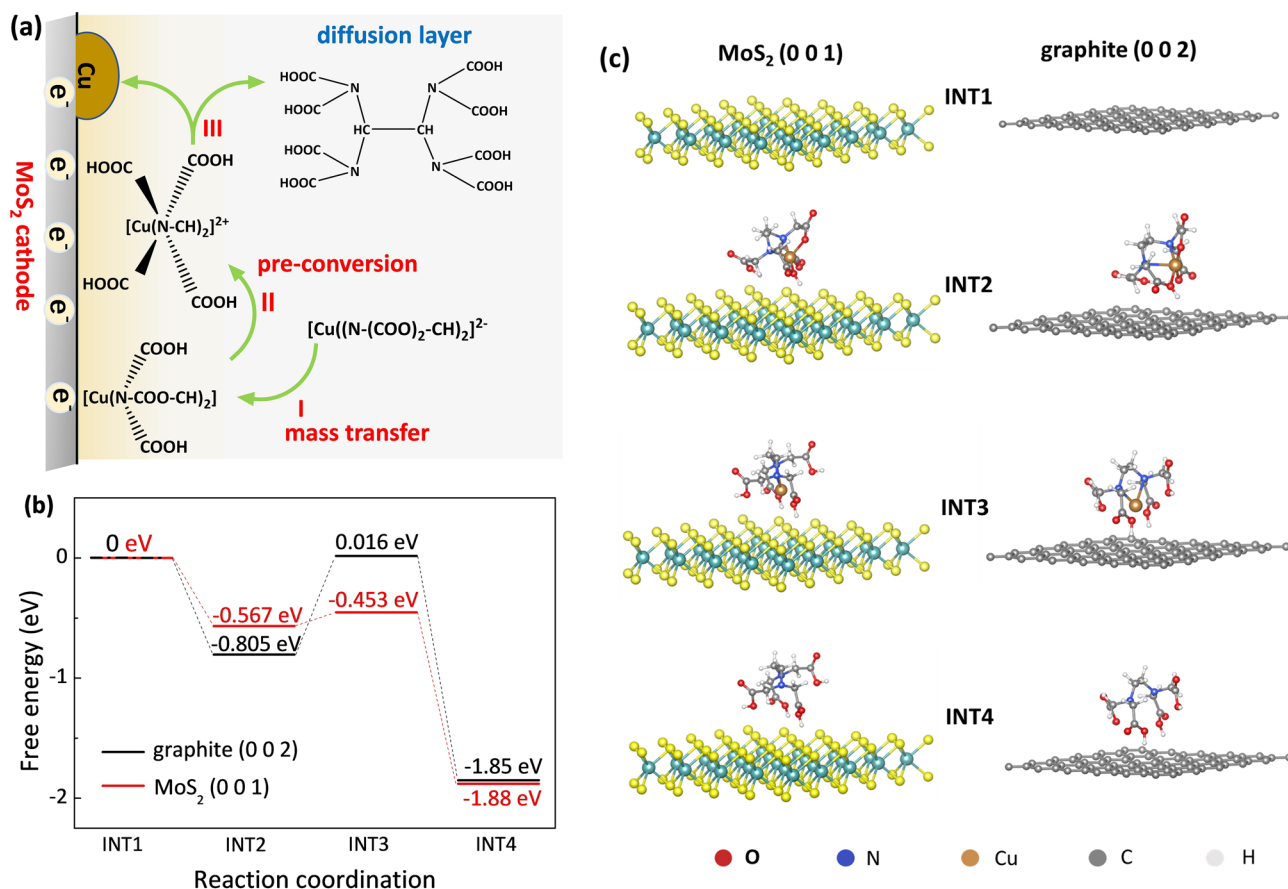
Fig. 4 **a** Schematic diagram of electrocatalytic reduction of CuEDTA at the MoS$_2$ cathode. **b** Energy states of different CuEDTA conformations on the MoS$_2$ (1 0 0) and graphite (0 0 2) surfaces. **c** Modeling of the CuEDTA reduction on the MoS$_2$ and graphite surface in the reaction process. INT1 to INT4 represent four reaction states of CuEDTA from 6 to 0 coordination

the existence of the vacant orbital is necessary to achieve the reduction of the central metal ion, which is the pre-conversion process. The pre-conversion process largely determines the overall efficiency of the CuRR, in which the decomplexation reaction of CuEDTA on the cathode can be expressed by the following equations:

$$CuEDTA(6) \rightarrow CuEDTA(4) \tag{1}$$

$$CuEDTA(4) \rightarrow CuEDTA(2) \tag{2}$$

$$CuEDTA(2) \rightarrow Cu^{2+} + EDTA^{2-} \tag{3}$$
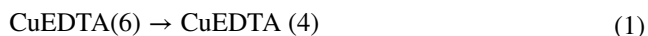
where the numbers in parentheses represent the coordination numbers of Cu^{2+}.

To understand how the MoS$_2$ nanosheets catalyze the CuRR process, DFT calculation was utilized to investigate the multi-step decomplexation process in CuEDTA

reduction (Text S6). The change of free energy of CuEDTA in the pre-conversion process on the MoS$_2$ surface and graphite surface was calculated for comparison (Fig. 4c). As shown in Fig. 4b, we stipulate that the initial energy of six-coordinated Cu on the (1 0 0) crystal plane of MoS$_2$ and the (0 0 2) crystal plane of graphite is 0 eV. Because of the Jahn–Teller effect, the energy that is needed for the CuEDTA to transform to the tetra-coordination state is decreased, which means that the transform of CuEDTA from 6 to 4 coordination is a spontaneous process. In contrast, the activation free energy of CuEDTA from four-coordinated to two-coordinated Cu is 0.821 eV for graphite and 0.114 eV for MoS$_2$ nanosheet, respectively. This result clearly indicates that the energy required for the decomplexation of CuEDTA on the MoS$_2$ surface is much lower than that on the graphite surface; thus, the speed of this step on the MoS$_2$ cathode is faster than that on the carbon cathode. The DFT

calculation results conform the inherent high activity of MoS$_2$ nanosheet for the decomplexation of CuEDTA, which theoretically support that the MoS$_2$ nanosheet cathode is suitable for electrochemical reduction removal of CuEDTA. This result also indicates that, for the electrochemical reduction removal of heavy metal complexes, the catalyst with low energy barrier for the conformation change of the complex is critical for the efficient reduction of heavy metal complexes.

3.3 CuEDTA Removal in Electrolyzer

In view of the excellent activity and selectivity of MoS$_2$ nanosheet for CuRR, two proof-of-concept devices were constructed to investigate the practical application prospects of CuEDTA removal, which is the electrolyzer for CuEDTA removal and the CuEDTA-Zn battery (MoS$_2$/GF, CuEDTA (SO$_4^{2-}$)‖OH$^-$, Zn) for simultaneous Cu removal and energy output. The electroreduction removal of CuEDTA wastewater in the electrolyzer was first investigated. The CuEDTA can be directly removed by anodic oxidation at the oxygen evolution potential window according to previous report [36–38]. Therefore, in order to eliminate the interference of anodic electrooxidation, the two-chamber electrolyzer was used. Different cathodes including MoS$_2$/GF, Ti, and GF were studied and compared in the electrolyzer. As shown in Fig. 5a, under good mass transfer condition by forced convection, CuEDTA can be removed fast with 84% removal rate in 10 min with the MoS$_2$/GF cathode, which is much higher than the Ti plate (40% removal rate in 10 min) that was commonly adopted as the cathode [11, 18], and is also higher than that of the GF cathode. The high removal rate of CuEDTA by the MoS$_2$/GF cathode further confirms that the MoS$_2$ nanosheet has outstanding catalytic performance in CuRR.

The potentiostatic method was adopted to further study the mass-transfer controlled removal process. In the experiment, three different cathodic potentials of −0.65, −0.70, and −0.75 V (vs. SCE) were applied. At these potentials, the removal rates of CuEDTA are almost the same as shown in Fig. 5b. The results match well with the electrochemical characterization results, which indicate that the mass transfer rate determines the CuRR process in the applied potential range. The current density of the cathode at three different cathodic potentials were also recorded (Fig. S8). The HER current density reaches the stable status rapidly after

the transient unstable electrode process (capacitor charging current and Faraday reaction current); while the CuRR current density gradually decreases. The reason for the CuRR current drop can be understood by the following dynamic equation of mass transfer-controlled electrode process:

$$j = nFD\frac{c - c_s}{l} \tag{4}$$

where C is the reactant concentration in solution, C_s is reactant concentration at electrode surface, n is the electron transfer number, F is the Faraday constant, D is the diffusion coefficient of CuEDTA, l is the thickness of the diffusion layer. As the reactant concentration, i.e., the CuEDTA concentration, decreases, the current density decreases. When the current density of CuRR becomes zero, the remaining cathode current is attributed to the HER current. It is found that the current densities are close under the applied cathodic potentials, which matches with the CuEDTA removal rates under different cathodic potentials (Fig. 5b).

The electroreduction of CuEDTA is an unstable or unsustainable process due to the coverage of the MoS$_2$/GF cathode by Cu deposition. To evaluate the durability of the cathode, the recycling test was carried out. As shown in Fig. 5c, after 3 cycles, a degradation of the cathode performance is noticed. The SEM images of the cathode surface after the reaction confirm the deposition and coverage of Cu on the cathode (Fig. S9). The Cu-deposited electrode can be refreshed in saturated ethylene diamine tetraacetic acid, and its catalytic activity for CuEDTA removal can be fully recovered as shown in the 4th cycle. The above results show that the reported MoS$_2$/GF cathode has good practical application potential for CuEDTA wastewater treatment.

Furtherly, we investigated the impact of coexist chemicals in real environment water on the CuEDTA removal efficiency of our system. As shown in Fig. S10, it is found that the removal efficiencies of CuEDTA in tap water and pure water are almost the same; while the removal efficiency in surface water (100% CuEDTA removal in 10 min) is even higher. The results show that the coexist chemicals in tap water and surface water have no inhibiting effect on CuEDTA removal, demonstrating the potential of the system for practical environmental application. In addition to CuEDTA, we also measured the EDTA concentration during the electrochemical reduction process (Fig. S11). The results show that the ligand EDTA in
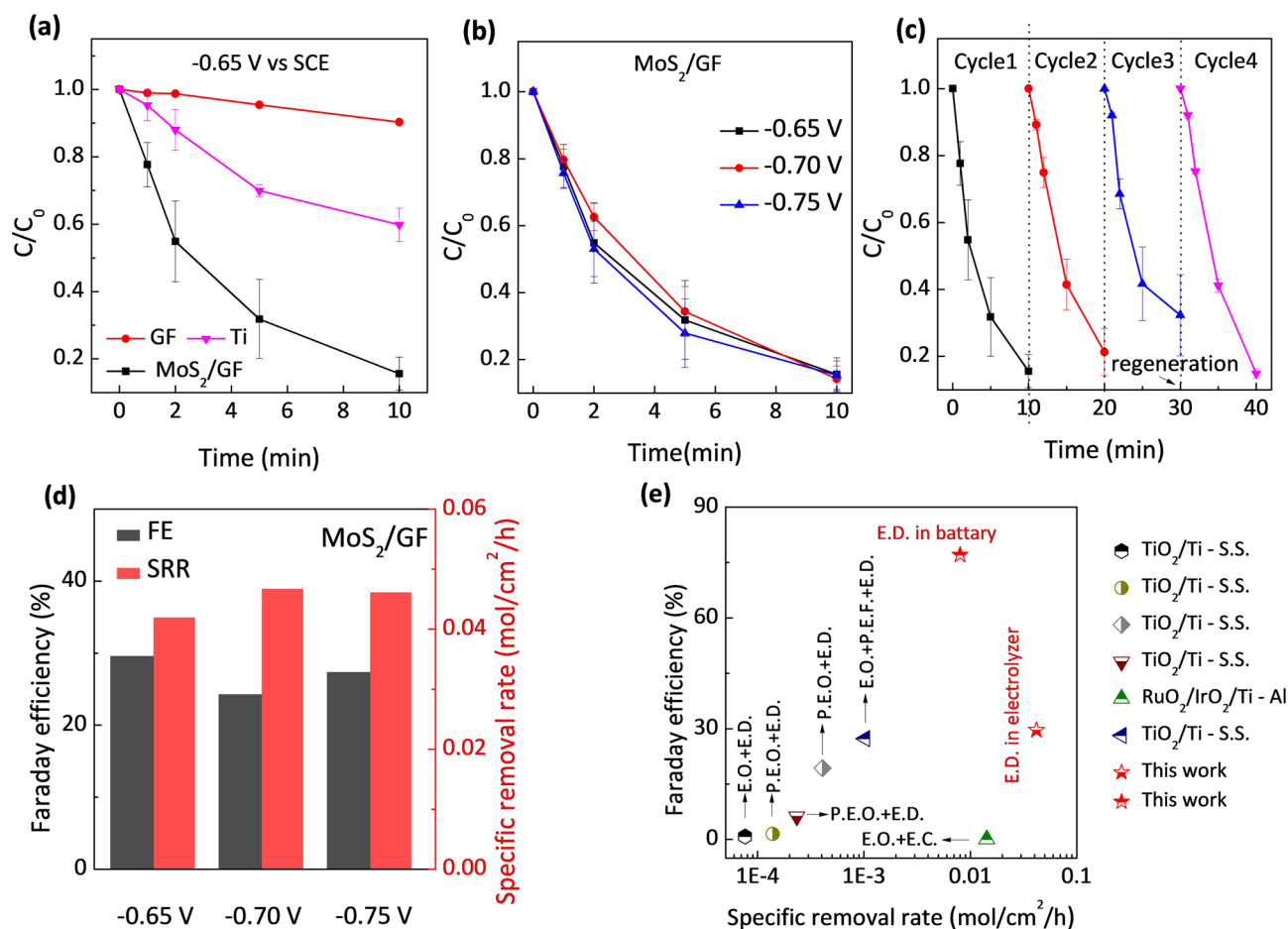
Fig. 5 Removal performance of CuEDTA **a** by MoS_2/GF, GF, and Ti cathodes; and **b** at different operation potentials by MoS_2/GF cathode. **c** Reusability of the MoS_2/GF cathode. **d** Faraday efficiency and special removal rate at different potentials with the MoS_2/GF cathode. Working condition: 1 mM CuEDTA, 0.5 M Na_2SO_4, 30 mL solution, 3 cm^2 electrode surface area. **e** Comparison of the FE and SRR of our MoS_2/GF system with other reported electrooxidation-based CuEDTA removal systems (E. represents electro, P. represents photo, O. represents oxidation, D. represents deposition, C. represents coagulation, F. represents Fenton, and S.S represents stainless steel)

CuEDTA remains unchanged during the electrode reaction process. The ligands alone are not toxic and can be further processed through inexpensive biological processes or recycled as industrial products. These results further demonstrate the potential of the system for practical environmental applications.

By integrating the chronoamperometric curve, the FE of CuEDTA removal at different potentials was obtained (Text S4). The specific removal rate (SRR) and FE of the MoS_2/GF cathode at the applied potentials are close, mainly due to the mass transfer limitation and the high selectivity for CuRR of MoS_2 nanosheet (Fig. 5d). The FE of the MoS_2/GF cathode in CuEDTA removal reaches 29.6% at the cathodic

potential of -0.65 V, while the highest SRR is obtained at 0.042 mol cm^{-2} h^{-1}. In order to demonstrate the superiority of the MoS_2/GF-based electrochemical deposition (E.D.) system, the FE and SRR values of this system were compared with other electrooxidation-based coupling systems (Fig. 5e) [3, 9, 31, 39, 40]. The electrochemical reduction system based on MoS_2/GF cathode is superior to the reported coupling systems based on electrooxidation, electrodeposition, photo-electrooxidation, electrocoagulation, and Fenton combined electrodeposition. Specially, the removal efficiency of the MoS_2/GF-based electrochemical deposition system is one to three orders of magnitude higher than those of the reported systems (see details in Table S1).

3.4 CuEDTA Removal in Zn-CuEDTA Battery

In another demonstrated system, we constructed a CuEDTA-Zn battery with MoS_2/GF as the cathode and Zn as the anode. The galvanic cell device not only can remove the CuEDTA, but also realizes the output of electric energy. The electrode reactions involving the Zn-CuEDTA battery are shown as follows:

$$\text{Anode:} \quad Zn - 2e^- = Zn^{2+} \tag{5}$$

$$\text{Cathode:} \quad CuEDTA + 2e^- = Cu + EDTA^{2-} \tag{6}$$
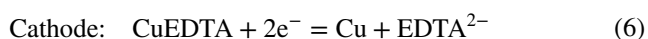
As shown in Fig. 6a, the as-built Zn-CuEDTA battery delivers a maximum power density (10 mM CuEDTA) of 1.05 mW cm^{-2} at 1.95 mA cm^{-2} by the MoS_2/GF electrode. In contrast, only 0.50 mW cm^{-2} of maximum power density is achieved at 1.35 mA cm^{-2} by the GF electrode. The output current density of the MoS_2/GF electrode with even

1 mM CuEDTA is also larger than that without CuEDTA (Fig. S12), confirming that the battery performance depends on the CuEDTA reduction reaction. The output performance of our Zn-CuEDTA battery can reach the level of Zn-NO batteries, exceeding the level of some reported Zn-CO_2 and Zn-N_2 batteries (Table S2).

The simultaneous CuEDTA removal and output performance of MoS_2/GF and GF electrodes at 0.5 mA cm^{-2} current density are shown in Figs. 6b and S13, respectively. The output voltage of the battery decreases gradually for both MoS_2/GF and GF electrodes along the discharge process. This decrease can be attributed to two reasons. Firstly, the concentration polarization gradually increases due to the decrease of CuEDTA concentration (removal of CuEDTA) in the battery discharge process. Secondly, the deposition of Cu on the electrode surface leads to the electrode deactivation. By integrating the voltage-charge curve, we calculated the cumulative electrical output of the Zn-CuEDTA battery.
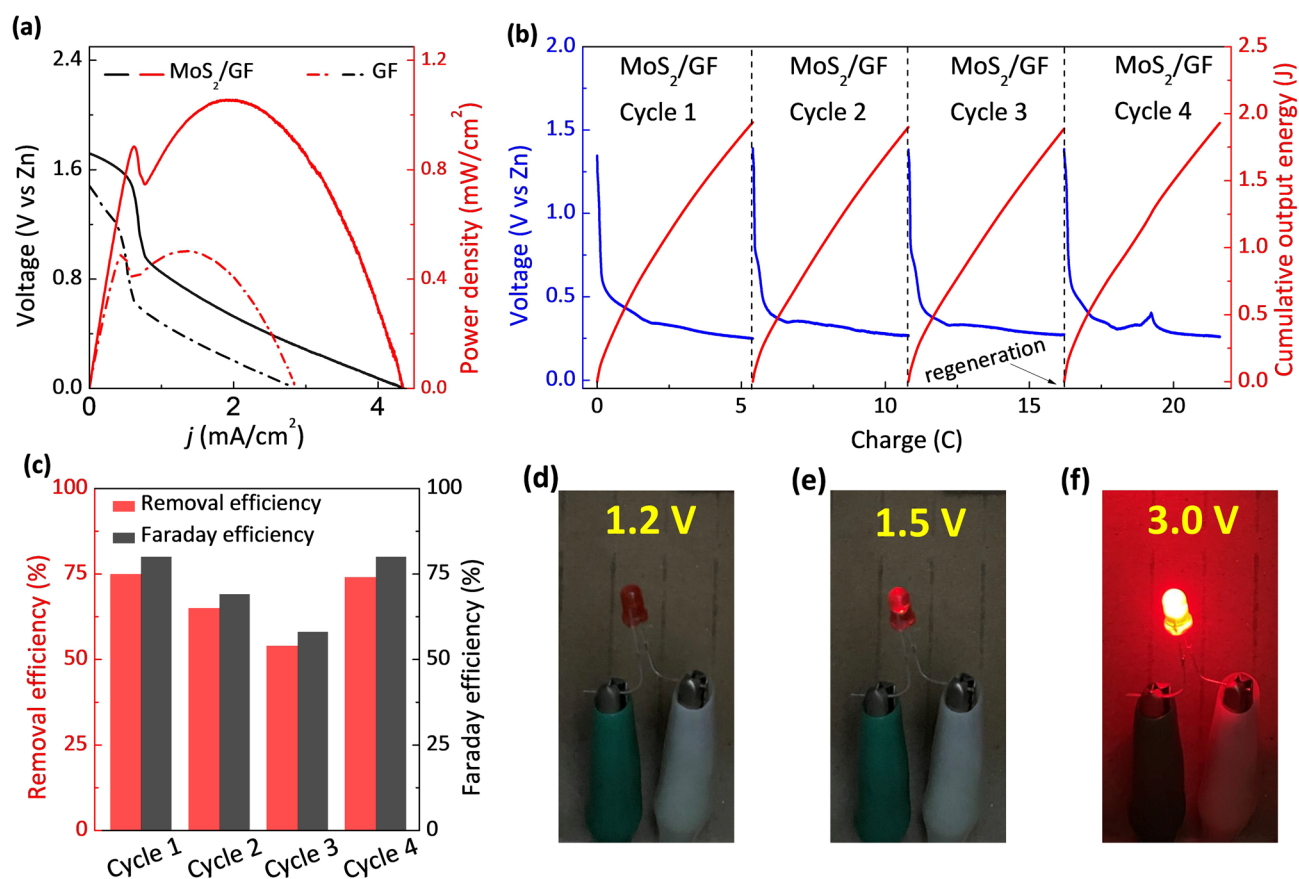
Fig. 6 a Polarization curve and power density plots of MoS_2/GF and GF-based batteries (10 mM CuEDTA). b Voltage and cumulative output energy at 0.5 mA cm^{-2} discharging density of MoS_2/GF-based battery in cycling test (1 h/cycle). c Removal efficiency and Faraday efficiency of MoS_2/GF-based battery. Working condition: 1 mM CuEDTA, 0.5 M Na_2SO_4, 30 mL solution, 3 cm^2 electrode area. d–f 20 mW LED light powered by the CuEDTA (1 or 10 mM)‖Zn (OH$^-$, 1 M) battery with output potentials of 1.2, 1.5, and 3.0 V

In 1 h of discharge, the battery with the MoS$_2$/GF electrode outputs 1.9 J; while the battery with the GF electrode outputs 0.6 J only.

For the battery's cycling test, in the first three cycles, the FE and removal efficiency of the battery with MoS$_2$/GF electrode gradually decrease. However, by using the same regeneration method, the FE and removal efficiency of the battery can be well recovered, as show in Fig. 6c. It is noticed that the battery with MoS$_2$/GF electrode has an outstanding FE of 77%, which is several times higher than the other reported systems in CuEDTA removal (Fig. 5e). The above results indicate that the MoS$_2$/GF electrode has high electrical output performance in CuEDTA-Zn battery, which is attributed to the excellent catalytic performance of MoS$_2$ nanosheet in CuRR.

To demonstrate the power output characteristic of the CuEDTA-Zn battery, a 20 mW LED light was powered by the Zn-CuEDTA battery. It is found that the bulb does not emit light when the battery is constructed with 1 mM CuEDTA electrolyte (Fig. 6d). However, by increasing the concentration of CuEDTA to 10 mM, the LED light can be lit (Fig. 6e). Through putting batteries in series, the LED light emits much stronger light (Fig. 6f). The LED light experiment further confirms the power output characteristic of the Zn-CuEDTA battery and demonstrates that the higher electrical power output can be obtained by higher CuEDTA concentration in actual CuEDTA wastewater treatment. The above results show that the prepared MoS$_2$/GF electrode has a practical application potential in CuEDTA-Zn battery for efficient pollutant removal and simultaneous power output.

4 Conclusion

In this study, MoS$_2$ nanosheet-based electrode was demonstrated in both electrolyzer and CuEDTA-Zn battery for highly efficient CuEDTA removal. The electrolyzer with MoS$_2$/GF cathode has a specific removal rate up to 0.042 mol cm^{-2} h^{-1} and Faraday efficiency of 29.6%. On the other hand, the CuEDTA-Zn battery based on MoS$_2$/GF electrode can simultaneously remove CuEDTA and deliver electric power output with a 1.05 mW cm^{-2} maximum energy density in 10 mM CuEDTA solution at 1.95 mA cm^{-2} current density. The battery with MoS$_2$/GF cathode has a super-high Faraday efficiency of 77% at 0.5 mA cm^{-2} discharge current density. Both systems achieve superior performances

in terms of the Faraday efficiency and specific removal rate than those of the other reported electrooxidation-based systems. The density functional theory modeling confirms that the activation energy of CuRR on the MoS$_2$ nanosheet surface is much lower than that of the other electrode, which explains the high activity and selectivity of MoS$_2$ in CuRR. This study not only reports an efficient electrochemical reduction system for metal complex pollutant removal but also a potential electrocatalytic system for simultaneous metal complex pollutant removal and energy output.

Declarations

References

1. W. Guan, B. Zhang, S. Tian, X. Zhao, The synergism between electro-Fenton and electrocoagulation process to remove Cu-EDTA. Appl. Catal. B-Environ. **227**, 252–257 (2018). https://doi.org/10.1016/j.apcatb.2017.12.036
2. M. Pan, C. Zhang, J. Wang, J.W. Chew, G. Gao et al., Multifunctional piezoelectric heterostructure of BaTiO$_3$@graphene: decomplexation of Cu-EDTA and recovery of Cu. Environ.

Sci. Technol. **53**(14), 8342–8351 (2019). https://doi.org/10.1021/acs.est.9b02355

3. X. Zhao, L. Guo, J. Qu, Photoelectrocatalytic oxidation of Cu-EDTA complex and electrodeposition recovery of Cu in a continuous tubular photoelectrochemical reactor. Chem. Eng. J. **239**, 53–59 (2014). https://doi.org/10.1016/j.cej.2013.10.088

4. Y. Zhu, W. Fan, T. Zhou, X. Li, Removal of chelated heavy metals from aqueous solution: a review of current methods and mechanisms. Sci. Total Environ. **678**, 253–266 (2019). https://doi.org/10.1016/j.scitotenv.2019.04.416

5. H. Zeng, S. Tian, H. Liu, B. Chai, X. Zhao, Photo-assisted electrolytic decomplexation of Cu-EDTA and Cu recovery enhanced by H_2O_2 and electro-generated active chlorine. Chem. Eng. J. **301**, 371–379 (2016). https://doi.org/10.1016/j.cej.2016.04.006

6. T. Wang, Y. Cao, G. Qu, Q. Sun, T. Xia et al., Novel Cu(II)-EDTA decomplexation by discharge plasma oxidation and coupled Cu removal by alkaline precipitation: underneath mechanisms. Environ. Sci. Technol. **52**(14), 7884–7891 (2018). https://doi.org/10.1021/acs.est.8b02039

7. T. Wang, Q. Wang, H. Soklun, G. Qu, T. Xia et al., A green strategy for simultaneous Cu(II)-EDTA decomplexation and Cu precipitation from water by bicarbonate-activated hydrogen peroxide/chemical precipitation. Chem. Eng. J. **370**, 1298–1309 (2019). https://doi.org/10.1016/j.cej.2019.04.005

8. S.S. Lee, H. Bai, Z. Liu, D.D. Sun, Green approach for photocatalytic Cu(II)-EDTA degradation over TiO_2: toward environmental sustainability. Environ. Sci. Technol. **49**(4), 2541–2548 (2015). https://doi.org/10.1021/es504711e

9. H. Zeng, S. Liu, B. Chai, D. Cao, Y. Wang et al., Enhanced photoelectrocatalytic decomplexation of Cu-EDTA and Cu recovery by persulfate activated by UV and cathodic reduction. Environ. Sci. Technol. **50**(12), 6459–6466 (2016). https://doi.org/10.1021/acs.est.6b00632

10. Y. Cao, X. Qian, Y. Zhang, G. Qu, T. Xia et al., Decomplexation of EDTA-chelated copper and removal of copper ions by non-thermal plasma oxidation/alkaline precipitation. Chem. Eng. J. **362**, 487–496 (2019). https://doi.org/10.1016/j.cej.2019.01.061

11. X. Huang, Y. Xu, Y. Shan, X. Li, W. Zhang et al., Coupled Cu(II)-EDTA degradation and Cu(II) removal from acidic wastewater by ozonation: performance, products and pathways. Chem. Eng. J. **299**, 23–29 (2016). https://doi.org/10.1016/j.cej.2016.04.044

12. H. Rong, C. Zhang, Y. Sun, L. Wu, B. Lian et al., Electrochemical degradation of Ni-EDTA complexes in electroless plating wastewater using PbO_2–Bi electrodes. Chem. Eng. J. **431**, 133230 (2022). https://doi.org/10.1016/j.cej.2021.133230

13. Y. Sun, C. Zhang, H. Rong, L. Wu, B. Lian et al., Electrochemical Ni-EDTA degradation and Ni removal from electroless plating wastewaters using an innovative Ni-doped PbO_2 anode: optimization and mechanism. J. Hazard. Mater. **424**, 127655 (2022). https://doi.org/10.1016/j.jhazmat.2021.127655

14. Z. Xu, C. Shan, B. Xie, Y. Liu, B. Pan, Decomplexation of Cu(II)-EDTA by UV/persulfate and UV/H_2O_2: efficiency and

mechanism. Appl. Catal. B-Environ. **200**, 439–447 (2017). https://doi.org/10.1016/j.apcatb.2016.07.023

15. H. Qin, Z. Ye, X. Wei, X. Liu, X. Liu et al., Bifunctional electrolyzation for simultaneous organic pollutant degradation and hydrogen generation. ACS ES&T Eng. **1**(9), 1360–1368 (2021). https://doi.org/10.1021/acsestengg.1c00173

16. H. Qin, X. Wei, Z. Ye, X. Liu, S. Mao, Promotion of phenol electro-oxidation by oxygen evolution reaction on an active electrode for efficient pollution control and hydrogen evolution. Environ. Sci. Technol. **56**(9), 5753–5762 (2022). https://doi.org/10.1021/acs.est.1c08338

17. A. Eivazihollagh, J. Bäckström, M. Norgren, H. Edlund, Influences of the operational variables on electrochemical treatment of chelated Cu(II) in alkaline solutions using a membrane cell. J. Chem. Technol. Biotechnol. **92**(6), 1436–1445 (2017). https://doi.org/10.1002/jctb.5141

18. A. Eivazihollagh, J. Backstrom, M. Norgren, H. Edlund, Electrochemical recovery of copper complexed by DTPA and C_{12}-DTPA from aqueous solution using a membrane cell. J. Chem. Technol. Biotechnol. **93**(5), 1421–1431 (2018). https://doi.org/10.1002/jctb.5510

19. R.S. Juang, L.C. Lin, Efficiencies of electrolytic treatment of complexed metal solutions in a stirred cell having a membrane separator. J. Membr. Sci. **171**(1), 19–29 (2000). https://doi.org/10.1016/s0376-7388(99)00377-4

20. R.S. Juang, L.C. Lin, Electrochemical treatment of copper from aqueous citrate solutions using a cation-selective membrane. Sep. Purif. Technol. **22–3**(1–3), 627–635 (2001). https://doi.org/10.1016/s1383-5866(00)00168-4

21. R.S. Juang, L.C. Lin, Treatment of complexed copper(II) solutions with electrochemical membrane processes. Water Res. **34**(1), 43–50 (2000). https://doi.org/10.1016/s0043-1354(99)00112-8

22. M. Chhowalla, H.S. Shin, G. Eda, L.-J. Li, K.P. Loh et al., The chemistry of two-dimensional layered transition metal dichalcogenide nanosheets. Nat. Chem. **5**(4), 263–275 (2013). https://doi.org/10.1038/nchem.1589

23. Q.H. Wang, K. Kalantar-Zadeh, A. Kis, J.N. Coleman, M.S. Strano, Electronics and optoelectronics of two-dimensional transition metal dichalcogenides. Nat. Nanotechnol. **7**(11), 699–712 (2012). https://doi.org/10.1038/nnano.2012.193

24. M. Tursun, C. Wu, Vacancy-triggered and dopant-assisted NO electrocatalytic reduction over MoS_2. Phys. Chem. Chem. Phys. **23**(35), 19872–19883 (2021). https://doi.org/10.1039/d1cp02764f

25. L. Zhang, J. Liang, Y. Wang, T. Mou, Y. Lin et al., High-performance electrochemical NO reduction into NH_3 by MoS_2 nanosheet. Angew. Chem. Int. Edit. **60**(48), 25263–25268 (2021). https://doi.org/10.1002/anie.202110879

26. X. Li, T. Li, Y. Ma, Q. Wei, W. Qiu et al., Boosted electrocatalytic N_2 reduction to NH_3 by defect-Rich MoS_2 nanoflower. Adv. Energy Mater. **8**(30), 1801357 (2018). https://doi.org/10.1002/aenm.201801357

27. R. Li, J. Liang, T. Li, L. Yue, Q. Liu et al., Recent advances in MoS_2-based materials for electrocatalysis. Chem. Commun.

58(14), 2259–2278 (2022). https://doi.org/10.1039/d1cc04004a

28. T. Wang, D. Gao, J. Zhuo, Z. Zhu, P. Papakonstantinou et al., Size-dependent enhancement of electrocatalytic oxygen-reduction and hydrogen-evolution performance of MoS_2 particles. Chem. Eur. J. **19**(36), 11939–11948 (2013). https://doi.org/10.1002/chem.201301406

29. I.S. Amiinu, Z. Pu, X. Liu, K.A. Owusu, H.G.R. Monestel et al., Multifunctional Mo-N/C@MoS_2 electrocatalysts for HER, OER, ORR, and Zn-Air batteries. Adv. Funct. Mater. **27**(44), 1702300 (2017). https://doi.org/10.1002/adfm.201702300

30. J. Lee, J. Lim, C.-W. Roh, H.S. Whang, H. Lee, Electrochemical CO_2 reduction using alkaline membrane electrode assembly on various metal electrodes. J. CO_2 Util. **31**, 244–250 (2019). https://doi.org/10.1016/j.jcou.2019.03.022

31. P. Song, C. Sun, J. Wang, S. Ai, S. Dong et al., Efficient removal of Cu-EDTA complexes from wastewater by combined electrooxidation and electrocoagulation process: Performance and mechanism study. Chemosphere (2022). https://doi.org/10.1016/j.chemosphere.2021.131971

32. Q. Xiang, J. Yu, M. Jaroniec, Synergetic effect of MoS_2 and graphene as cocatalysts for enhanced photocatalytic H_2 production activity of TiO_2 nanoparticles. J. Am. Chem. Soc. **134**(15), 6575–6578 (2012). https://doi.org/10.1021/ja302846n

33. L. Zhang, J. Liang, Y. Wang, T. Mou, Y. Lin et al., High-performance electrochemical NO reduction into NH_3 by MoS_2 nanosheet. Angew. Chem. Int. Edit. **60**(48), 2110879 (2021). https://doi.org/10.1002/anie.202110879

34. B. Zong, Q. Li, X. Chen, C. Liu, L. Li et al., Highly enhanced gas sensing performance using a 1T/2H heterophase MoS_2 field-effect transistor at room temperature. ACS Appl. Mater. Interfaces **12**(45), 50610–50618 (2020). https://doi.org/10.1021/acsami.0c15162

35. S. Sarma, S.C. Ray, Magnetic behaviors of single crystal-MoS_2 (MoS_2-SC) and nanoparticle-MoS_2 (MoS_2-NP) and bi-layer-MoS_2 thin film. J. Magn. Magn. Mater. **546**, 168863 (2022). https://doi.org/10.1016/j.jmmm.2021.168863

36. P. Song, C. Sun, J. Wang, S. Ai, S. Dong et al., Efficient removal of Cu-EDTA complexes from wastewater by combined electrooxidation and electrocoagulation process: performance and mechanism study. Chemosphere **287**, 131–971 (2022). https://doi.org/10.1016/j.chemosphere.2021.131971

37. J. Xie, J. Ma, S. Zhao, T.D. Waite, Flow anodic oxidation: towards high-efficiency removal of aqueous contaminants by adsorbed hydroxyl radicals at 1.5 V vs SHE. Water Res. **200**(2021). https://doi.org/10.1016/j.watres.2021.117259

38. J. Xie, C. Zhang, T.D. Waite, Hydroxyl radicals in anodic oxidation systems: generation, identification and quantification. Water Res. **217**, 118425 (2022). https://doi.org/10.1016/j.watres.2022.118425

39. X. Zhao, L. Guo, B. Zhang, H. Liu, J. Qu, Photoelectrocatalytic oxidation of Cu-II-EDTA at the TiO_2 electrode and simultaneous recovery of Cu-II by electrodeposition. Environ. Sci. Technol. **47**(9), 4480–4488 (2013). https://doi.org/10.1021/es3046982

40. X. Zhao, J. Zhang, J. Qu, Photoelectrocatalytic oxidation of Cu-cyanides and Cu-EDTA at TiO_2 nanotube electrode. Electrochim. Acta **180**, 129–137 (2015). https://doi.org/10.1016/j.electacta.2015.08.103